Hydro-Geomorphic Diagnosis of a Rainfall-Induced Landslide in Davao City, Philippines: Implications for Community Resilience

Lester G. Padilla* and Eleonor V. Palconit

School of Engineering and Architecture, Ateneo de Davao University, Davao City, Philippines
Email: lesterpadilla1993@gmail.com, lgpadilla@addu.edu.ph (L.G.P); evpalconit@addu.edu.ph (E.V.P)
*Corresponding author

Manuscript received October 07, 2025; revised November 19, 2025; accepted December 9, 2025; published April 7, 2026

Abstract*—Rainfall-induced landslides pose a significant threat to tropical mountain roads, where the interaction of hydrological loading, geomorphic development, and soil weakening drives failure. This study presents an integrated hydro-geomorphic diagnosis of the July 2022 Callawa–Fatima landslide in Davao City, Philippines, by combining field surveys, drone photogrammetry, historical satellite imagery, Digital Elevation Models (DEMs), rainfall records, and numerical slope stability modeling. Multi-temporal analysis revealed a tensile crack along the ridge crest as early as 2015, while 5-m contour interpretation highlighted topographic irregularities that signaled long-term geomorphic preconditioning. Hydrological assessment based on rainfall data revealed that several days of antecedent wetting, from July 8 to 12, 2022, saturated the slope before the short-duration, high-intensity rainfall on July 13-14, 2022, triggered the failure. Catchment modeling in Quantum Geographic Information System (QGIS): Geographic Resources Analysis Support System (GRASS) module confirmed concentrated flow paths converging toward the failure zone. Limit-equilibrium simulations conducted in GEO5 demonstrated that the slope was already marginally unstable under dry-season conditions with Factor of Safety, FoS≈0.87–1.35, and transitioned to global instability under rainfall-induced pore-pressure loading with FoS ≈ 0.58–0.76. During the spatial exposure, QGIS deep-learning mapping, identified house location along the active scarps as directly exposed and downstream community as indirectly at risk. The integrated framework offers a cost-effective and transferable approach for diagnosing rainfall-induced slope failures and enhancing community resilience in tropical mountain regions.

***Keywords*—hydro-geomorphic diagnosis, catchment hydrology, slope stability, tropical mountain roads, community resilience**

I. Introduction

Mountain road networks in tropical regions are highly vulnerable to rainfall-induced slope failures, which frequently disrupt transportation, damage infrastructure, and endanger nearby communities [1, 2]. These hazards are not isolated events but the cumulative result of interacting hydrological, geomorphic, and geotechnical processes [3]. In clay-rich terrains, particularly those shaped by steep volcanic and sedimentary deposits, even moderate rainfall can trigger instability once soils have become saturated [4]. Such events underscore the need for integrated assessments that transcend single-discipline approaches, linking rainfall dynamics, topographic evolution, and soil strength behavior to understand pathways from preconditioning to collapse [3, 5].

Globally, rainfall-induced landslides are projected to intensify under a changing climate, as extreme precipitation events become more frequent and prolonged [6, 7]. In Southeast Asia, and particularly in the Philippines, this challenge is exacerbated by the vulnerability of critical infrastructure and densely populated settlements along mountainous corridors [8]. Despite numerous engineering and hazard mapping efforts, gaps remain in characterizing how short rainfall sequences, antecedent wetness, and drainage convergence combine with dormant geomorphic features to produce slope failures [9]. In the absence of an integrated understanding, risk reduction efforts tend to remain reactive rather than preventive, leaving communities vulnerable to repeated disasters [10].

Equally important, the societal dimension of slope failures has received limited attention in technical studies [10]. In many mountain communities, households remain near active scarps, tension cracks, and compression ridges despite recurring signs of instability [11]. Such proximity not only magnifies immediate risk but also complicates long-term recovery and risk communication [12]. A comprehensive diagnostic framework must therefore consider not only hydro-geomorphic processes but also human–landscape interactions to ensure relevance for disaster preparedness and resilience strategies [13]. Comparable issues were observed in the mountainous regions of India, where, despite extensive scientific research and hazard mapping, the limited dissemination of critical knowledge to local communities continues to hinder effective preparedness [14].

While previous research has advanced the understanding of rainfall-induced slope instability, most studies have examined geotechnical or hydrological factors separately [15], with limited integration of geomorphic evolution and community exposure aspects [16]. Furthermore, regional investigations within the Philippines remain scarce, and few have combined field-based geomorphic mapping, rainfall-runoff assessment, and numerical stability modeling into a unified diagnostic framework [8]. This gap restricts the ability to anticipate slope behavior under varying rainfall conditions and to translate scientific findings into actionable resilience measures for mountain road networks.

This study, therefore, aims to establish a comprehensive hydro-geomorphic diagnostic framework for the Callawa–Fatima landslide. Specifically, it integrates (i) geomorphic analysis of historical imagery and topographic data, (ii) hydrological assessment of rainfall and catchment delineation, (iii) numerical modeling of slope stability under both dry-season and rainfall-influenced hydrological scenarios, and (iv) spatial household vulnerability mapping and exposure assessment. Unlike conventional slope studies, which treat hydrological, geomorphic, and geotechnical

analyses separately, this research introduces an integrated workflow that quantitatively links rainfall sequences, catchment hydrology, and slope stability modeling using accessible, open-source tools. Its novelty lies in combining physical process diagnosis with community exposure mapping, thereby translating technical slope assessments into actionable insights for road safety and resilience planning in tropical mountain regions. Beyond reconstructing a single landslide event, the Callawa–Fatima case highlights the importance of hydro-geomorphic diagnostic tools in enhancing climate-resilient road infrastructure and mitigating vulnerability in rainfall-sensitive mountain regions. It also examines considerations related to the potential reactivation of the landslide and its possible extension into adjacent slopes.

II. Materials and Methods

A. Study Area

The study was conducted along the Callawa–Fatima Road section in Davao City, Mindanao, Philippines (7°16'44.02"N, 125°31'35.60"E), as illustrated in Fig. 1. The road, constructed on steep terrain underlain by weathered volcanic and sedimentary deposits, has remained closed to vehicular traffic since July 2022 following a rainfall-induced landslide. The failure zone was marked by a head scarp approximately 205m wide, tension cracks extending upslope, and disrupted drainage pathways, with the displaced mass encroaching on both the road embankment and the river toe. The site was further constrained by nearby households situated upslope and downslope of the failed section, underlining its dual significance as an engineering challenge and a community safety concern. These conditions make the Callawa–Fatima landslide an appropriate case for developing a hydro-geomorphic study that integrates geomorphic, hydrological, and geotechnical perspectives.

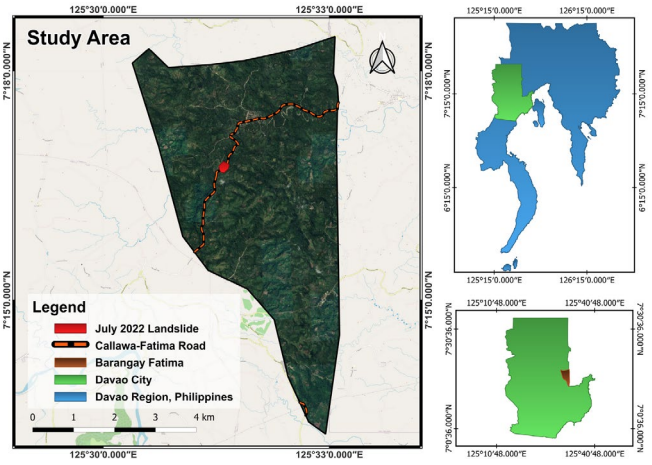

Fig. 1. The study area: Callawa-Fatima landslide section.

B. Methodological Framework

The overall methodological framework adopted in this study is summarized in Fig. 2. It integrates 5 primary analytical blocks and datasets, field observations with UAV remote sensing, rainfall and hydrological assessment, geomorphic evolution analysis, numerical slope stability modeling, and spatial household vulnerability and exposure assessment [17, 18]. Field evidence, multi-temporal satellite imagery, Digital Elevation Models (DEMs), rainfall hyetographs, and soil strength parameters were processed to generate inputs for hydrological, geomorphic, and numerical stability analyses [19, 20]. These analyses were implemented using QGIS (for hydrological and terrain functions), GRASS GIS (for catchment and drainage delineation), and GEO5 Slope Stability (for Limit Equilibrium Method) [21, 22]. The workflow linked input datasets with diagnostic outputs, including factors of safety, hydrological response, and modeled slope failure geometries, which were subsequently validated against field observations. Collectively, the framework provides an integrated hydro-geomorphic diagnostic for interpreting rainfall-induced slope failures and assessing their implications for community safety and resilience.

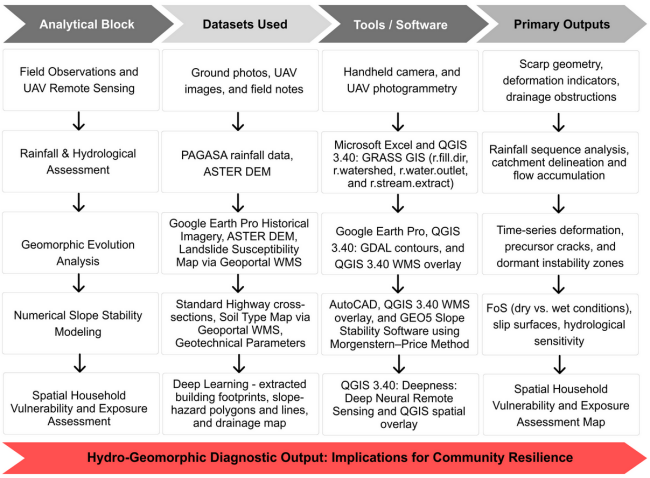

Fig. 2. Workflow of the hydro-geomorphic diagnostic assessment.

1) Field evidence analysis

Field evidence was obtained from reconnaissance surveys conducted immediately after the July 2022 failure and an Unmanned Aerial Vehicle (UAV) photogrammetric survey with ground validation, which was revisited on August 29, 2025 [23, 24]. The surveys involved systematic documentation of scarp geometry, road deformation, drainage conditions, vegetation stress, and other geomorphic indicators using georeferenced photographs and field notes [25]. Drone imagery was processed to generate high-resolution orthophotos and a 3D surface model of the failure zone [25]. These datasets were compiled to characterize slope conditions and provide inputs for subsequent hydro-geomorphic and stability analyses.

2) Hydrological analysis

The hydrological component focused on the rainfall sequence from July 8 to 15, 2022, which triggered the landslide. Three-hourly and daily rainfall data were acquired from the PAGASA Climate and Agrometeorological Data Section (CADS). Hyetographs were generated in Microsoft Excel to analyze rainfall intensity, and cumulative indices were computed at 3-hour intervals over 7 days to quantify antecedent wetness and to identify the peak rainfall event that triggered the landslide [26].

Terrain-based hydrological modeling was also carried out using Advanced Spaceborne Thermal Emission and Reflection Radiometer (ASTER) DEM data processed in QGIS 3.40 [27]. Depressions were corrected using the

GRASS GIS module r.fill.dir, and flow direction and accumulation grids were generated with r.watershed [21, 28]. Catchment boundaries were delineated using r.water.outlet, and stream networks were extracted using r.stream.extract [21, 28]. Catchment delineation identified two contributing sub-catchments and clarified the hydrological setting of the slope.

However, the ASTER DEM (30 m) resolution is too coarse for small-scale catchment modeling and microtopographic analysis [29]. The relatively coarse grid spacing can smooth subtle topographic variations, underestimate slope gradients, and generalize drainage pathways, particularly in steep, narrow terrain such as the Callawa–Fatima site [29]. Thus, this study acknowledged these limitations and recommended cross-checking the hydrological results with field validation data and geomorphic analysis to ensure consistency and reliability.

3) Geomorphic analysis

Geomorphic changes were reconstructed using multi-temporal satellite imagery from Google Earth Pro, spanning the years 2012–2023 [30, 31]. Images representing key stages of slope evolution (2012, 2015, 2018, 2019, 2021, 2022, and 2023) were analyzed to identify progressive development of scarps, cracks, and slope deformations [31].

Topographic interpretation employed ASTER DEM-derived contours at 20 m, 15 m, and 10 m and 5 m intervals using the Contour (GDAL) tool in QGIS 3.40 [27]. Coarser intervals highlighted overall slope morphology, while the finer 5 m contours revealed microtopographic features such as breaks, ridges, and depressions [32]. Additionally, a landslide susceptibility map was generated using the Philippine Geoportal platform, which integrates Web Map Service (WMS) in QGIS 3.40 [33]. The WMS layer was imported directly into the GIS environment to overlay hazard zoning with the DEM-derived slope features and field-mapped scarps [34]. This integrated approach, combining satellite-based temporal analysis with DEM-derived topographic interpretation and ground-truthing, provided a reconstruction of the geomorphic processes that culminated in the slope failure.

4) Numerical modeling

A soil map was also accessed from the Philippine Geoportal and incorporated into QGIS via WMS [34]. The classified soil unit corresponding to the study site was used to assign geotechnical properties, with conservative values selected to represent the material [35]. These parameters served as inputs for stability simulations in the GEO5 Slope Stability module. Slope stability analysis was conducted using the GEO5 Slope Stability module, which applies the Limit Equilibrium Method (LEM) [22, 35, 36]. A standard Philippine roadway cross-section was prepared in AutoCAD and exported as a .DXF file for import into GEO5.

The Morgenstern–Price method was adopted during simulations as it satisfies both force and moment equilibrium and allows a variable interslice force function, providing a rigorous assessment for complex slopes [37]. Other Limit Equilibrium formulations, such as the Bishop and Janbu methods, impose simplifying assumptions that reduce computational rigor [37]. Table 1 summarizes the comparative characteristics of these methods and justifies the selection of the Morgenstern–Price approach for this study [37, 38].

Table 1. Comparative characteristics of LEM

Method	Equilibrium Conditions	Assumptions / Limitations	Typical Use
Morgenstern–Price	Force + Moment equilibrium	Variable interslice force function	Complex, heterogeneous slopes
Bishop Simplified	Moment equilibrium; no interslice shear	Assumes circular slip; valid for uniform soils	Homogeneous circular failures
Janbu Simplified	Force equilibrium only	Does not ensure moment equilibrium	Embankments and simple slopes

The LEM was preferred over more advanced numerical techniques, such as the Finite Element Method (FEM), because it yields interpretable results with fewer input parameters and is well-suited for field-based diagnostics in data-limited contexts [38]. Although FEM offers a more detailed simulation of coupled stress–strain and pore-pressure behavior, its application is often constrained by the scarcity of site-specific constitutive and hydromechanical parameters in tropical residual soils [39]. Therefore, LEM ensured methodological consistency with the hydro-geomorphic diagnostic framework while remaining computationally efficient for slopes characterized by limited geotechnical information.

Lastly, two hydrological scenarios were evaluated [40, 41]. The first represented dry-season baseline conditions, characterized by a drained and unsaturated soil profile and a groundwater table deeper than 5 m [40, 41]. The second scenario simulated rainfall-induced infiltration by applying the pore pressure coefficient (r_u), which accounted for the influence of transient pore-water pressures on the reduction of shear strength [42, 43]. For both scenarios, the Factor of Safety (FoS) was calculated using the Morgenstern–Price method under the standard safety factor settings in GEO5 [44, 45].

1) Spatial household vulnerability mapping and exposure assessment

A household vulnerability exposure assessment was conducted to identify settlements that are potentially at risk from slope instability. This procedure integrated Deep Learning (DL) building detection [46], geomorphic mapping [47, 48], and hydrological flow analysis [49] to delineate households potentially affected by slope reactivation or debris-related hazards.

High-resolution satellite imagery was processed in QGIS 3.40 using the Deepness: Deep Neural Remote Sensing plugin to extract building footprints automatically [50]. The plugin performed deep neural inference on orthophotos and high-resolution imagery in ONNX format, enabling semantic segmentation of built structures [50]. Detected footprints were exported as vector layers.

Settlement footprints were classified as directly exposed when their locations spatially coincided with mapped hydro-geomorphic indicators of instability, including proximity to tensile cracks or documented failure zones, observable surface deformation, dense tributary convergence, or traces of past slope movements identified in historical imagery [51]. Indirect exposure, meanwhile, was assigned to settlements that did not intersect the primary hazard polygons

but were positioned along connected drainage pathways or adjacent slopes forming the broader impact domain, where secondary processes, such as debris runout or sediment inundation, may propagate following a primary failure [51].

III. Result and Discussion

A. Field Evidence Results

Field reconnaissance in July 2022 documented a major slope failure along the Callawa–Fatima Road, as shown in Fig. 3 below. The event created a steep head scarp that cut through the roadway and displaced debris downslope. Two hazards were evident: the main slide, which disrupted road access, and a landslide deposit that blocked the river, causing water to accumulate upstream. The affected section spanned roughly 205 meters, with tension cracks near the crown, indicating ongoing instability. These features illustrated how a single slope failure can trigger cascading impacts, paralyzing transport while simultaneously creating conditions for sudden debris flow that could endanger the nearby barangay of Fatima. The observations provided a critical baseline for subsequent stability analysis and the design of mitigation measures.

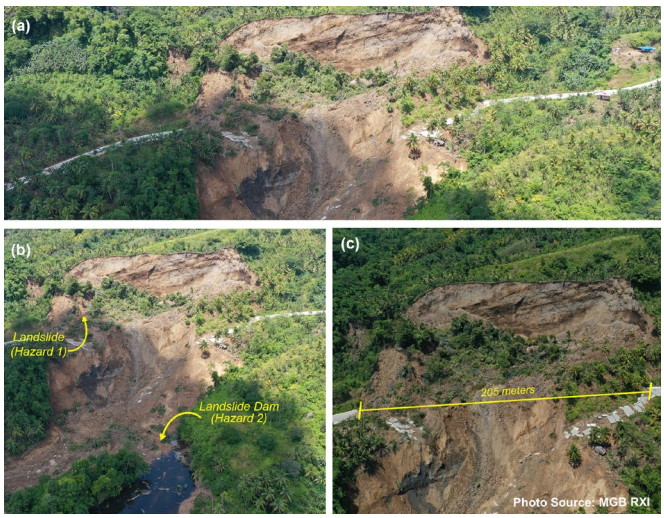

Fig. 3. Callawa-Fatima Landslide (a) Landslide head scarp and debris, (b) Main slide and landslide dam, (c) 205-m section with crown cracks.

A site inspection on July 11, 2022, as documented in Fig. 4, revealed visible signs of collapse. The roadway showed differential settlement (a), while tensile cracks traced the upper slope (b), marking the early stage of the main scarp. On the downslope side (c), a partial road slip exposed the cross-drain, which had already been damaged by ground movement. Vegetation stress was also evident, (d) with several leaning trees suggesting progressive displacement. Taken together, these observations confirmed that the slope was in a pre-failure state, with structural and geomorphic indicators pointing to imminent large-scale movement once additional rainfall occurred.

Fig. 4. Indicators of slope instability (a) roadway settlement & longitudinal cracks; (b) upslope tensile cracks; (c) downslope slip exposing cross-drain; (d) leaning trees (creep).

A drone-based photogrammetric survey was conducted on August 29, 2025, as shown in Fig. 5, which generated both a textured 3D model (a) and a triangular surface mesh (b) of the Callawa–Fatima landslide [52]. The textured model clearly illustrated the sharp head scarp, displaced debris, and partial vegetation recovery, while also distinguishing bare surfaces that remain unstable. In contrast, the triangular surface mesh highlighted the geometric detail of the slope, delineating crown cracks, downslope bulging, and irregular terrain associated with mass displacement. Together, these outputs confirmed that instability persists more than three years after the failure, with adjacent steep sections showing limited ground cover and high susceptibility to secondary movement.

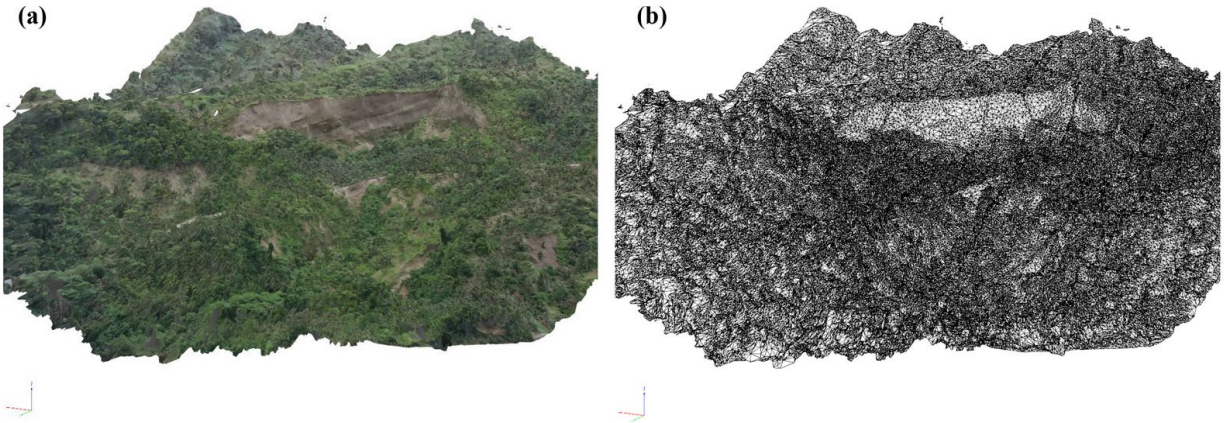

Fig. 5. UAV Photogrammetry (a) Textured 3D Model; (b) Triangular Surface Mesh.

Furthermore, the ground observation on August 29, 2025, confirmed that the landslide zone remains unstable, with the conditions documented in Fig. 6. The main scarp was still prominent, with banana growth observed along the middle

section of the collapsed section (a). Signs of continued movement included a leaning coconut tree with exposed roots (b) and additional bent trees downslope of the scarp (d). At the end of the landslide road section (c), the pavement was displaced and partly buried by soil and dense vegetation, marking the termination of the failed alignment.

Fig. 6. Ongoing slope movement indicators (a) main scarp with banana regrowth, (b) leaning coconut with exposed roots, (c) displaced pavement at one end of the collapsed road, and (d) bent trees downslope.

Fig. 7. Post-failure access and surface deformation (a) narrow improvised bypass at the failed section; (b) motorcycle crosses toward Barangay Fatima; (c) unpaved track with banana regrowth on the slide mass; (d) developing tensile crack along the path.

Additional ground evidence, as shown in Fig. 7, highlighted how the landslide site continues to impact mobility. At the start of the failed section (a), residents created a narrow detour that allowed only motorcycles to pass, cutting directly across the middle of the landslide zone just below the main scarp. A motorcycle passerby was observed using this route to reach Barangay Fatima (b), avoiding the longer alternate road. The detour remained unpaved, with banana growth visible in the middle of the landslide body (c). Lastly, a developing tensile crack was observed along this improvised pathway (d), indicating that the ground remained unstable even along the trail currently used by the community. These observations demonstrated the continued exposure of residents, who rely on this everyday passage despite the high risk of slope movement.

A. Hydrological Results

The rainfall record between July 8–15, 2022, showed a total accumulation of 33.04mm, with a maximum 3-hourly intensity of 11mm as illustrated in Fig. 8. Although the total rainfall was modest compared to extreme tropical storms, the event sequence illustrates how even moderate precipitation can destabilize saturated clay slopes.

On July 8–9, several millimeters of rainfall initiated slope wetting, aggravating the tensile cracks previously noted at the scarp. Despite no rain on July 10, residents reported early signs of slope distress, suggesting that infiltration and delayed pore-pressure rise had already weakened the soil matrix.

During July 11–12, only light rain (0.1mm ~ 0.80mm per 3 h) was recorded, coinciding with a government inspection that confirmed the presence of cracks and minor slope movement. These observations highlighted that slope instability can persist even under low rainfall when antecedent wetness remains high.

The critical moment occurred on July 13–14, when 3-hourly rainfall peaked at 11 mm, following several preceding bursts that exceeded 2.8mm ~ 5.6mm. This short but intense input elevated pore pressures within an already saturated slope, reducing shear strength and triggering the landslide. By July 15, rainfall had diminished to 0.40mm, but the slope had already failed.

This sequence highlighted a crucial hydrological mechanism: the progressive weakening from low to moderate antecedent rainfall, followed by collapse under a single, short-duration, high-intensity burst. Although the cumulative rainfall was not extreme, the timing and intensity distribution proved sufficient to exceed slope resistance. These findings were consistent with those from other tropical mountain slopes, where the timing and sequence of rainfall often matter more than total rainfall in triggering landslides.

Fig. 9 below presents the catchment delineation that clarified the hydrological setting of the Callawa–Fatima slope. The landslide body lay entirely within Catchment Area 1, which drained directly through the failed section, whereas Catchment Area 2 contributed flow to the downstream channel only indirectly. This distinction highlighted the dominant role of Catchment Area 1 in concentrating rainfall input toward the landslide zone.

The 3D hydrological catchment model depicted in Fig. 10 further illustrated how drainage converged in the vicinity of the July 2022 landslide. Minor tributary streams intersected the scarp area, providing a preferential pathway for infiltration. At the toe, the adjacent main river channel imposed an additional destabilizing influence by maintaining saturation and exerting erosional pressure. The combined effect of upslope convergence and toe loading created a critical hydrological imbalance during the July 2022 rainfall episode.

These findings emphasized that the landslide was not triggered solely by rainfall, but by the interaction of rainfall, catchment-scale flow concentration, and local drainage geometry. The slope's position along a watershed divide, with the road alignment crossing between two catchments, likely intensified the problem by altering natural runoff distribution and channeling excess flow into already weakened sections.

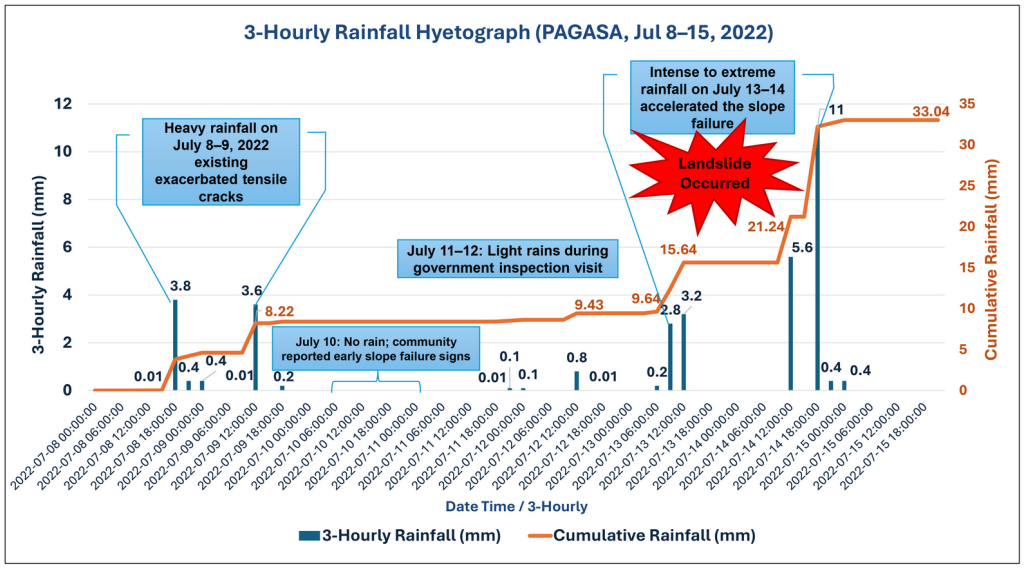

Fig. 8. 3-Hourly Rainfall Hyetograph (PAGASA, Jul 8–15, 2022).
Data Source: Climate and Agrometeorological Data Section (CADS), Philippine Atmospheric, Geophysical and Astronomical Services Administration (PAGASA)

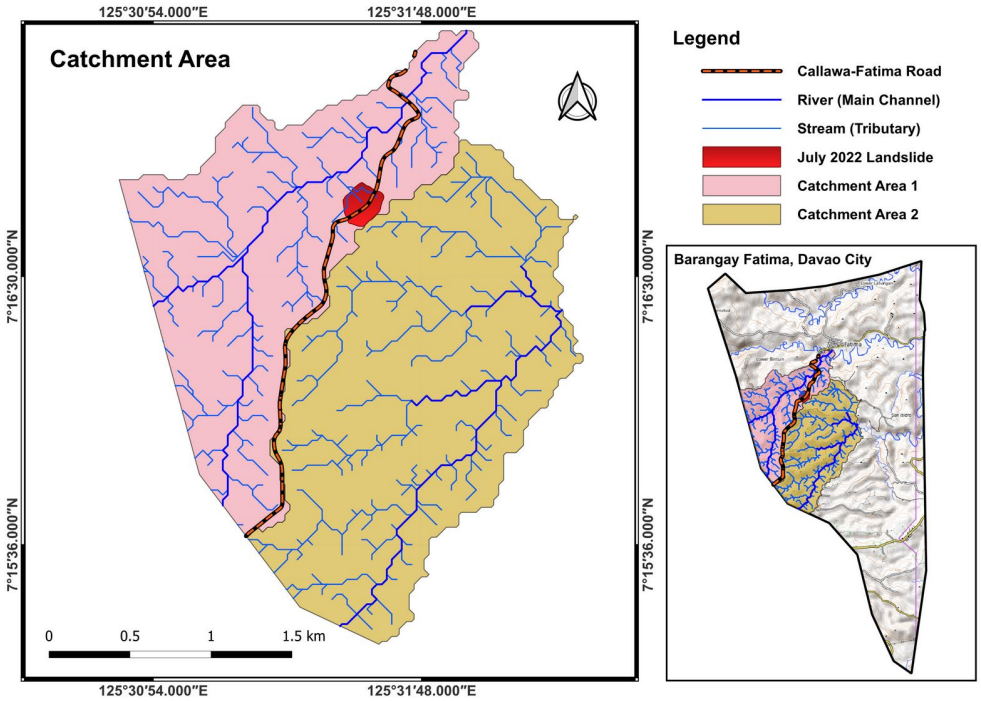

Fig. 9. Catchment Area 1 drains through the landslide zone; Catchment Area 2 flows indirectly downstream from the opposite slope.

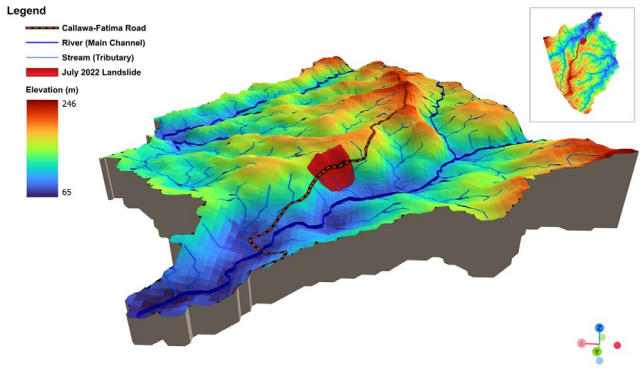

Fig. 10. 3D hydrological catchment model.

A. Geomorphic Results

The progressive development of the Callawa–Fatima landslide was also interpreted through contour-based terrain interpretation, portrayed in Fig. 11. The comparison of contour intervals (20 m, 15 m, 10 m, and 5 m) demonstrated how resolution affects the identification of slope instability features. Coarser intervals (20–15 m) captured the general slope geometry. Still, they obscured finer details, while the 10 m and especially the 5 m intervals revealed subtle variations in topography that are indicative of slope failure.

At the 5 m contour interval (a) as illustrated in Fig. 12 above, the July 2022 landslide body is sharply defined, with features such as a horseshoe-shaped scarp, crown cracks, downslope bulging, and compression ridges that align closely with established landslide topographic features (b). Notably, the adjacent east slope of the 2022 main scarp also exhibited a comparable set of topographic features of a landslide, including irregular contour deflections, crown-parallel tension cracks, and a concave depression zone. These characteristics are strongly suggestive of an older, inactive,

or dormant landslide body that has remained structurally weakened over time. Importantly, this section is underlain by a tributary stream upslope and bordered by the main river channel downslope, creating a dual hydrological influence that increases susceptibility to reactivation. The existing deformation features and hydrological forcing suggested that the adjacent slope may extend the 2022 landslide or form a secondary failure zone during future extreme rainfall events.

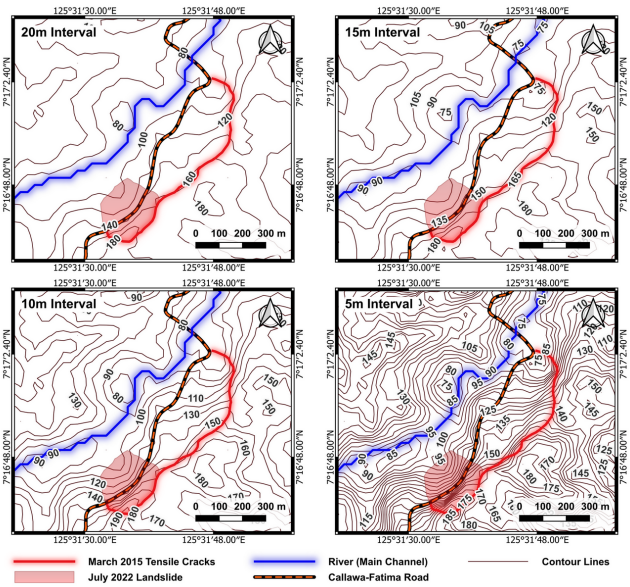

Fig. 11. Comparison of contour intervals.

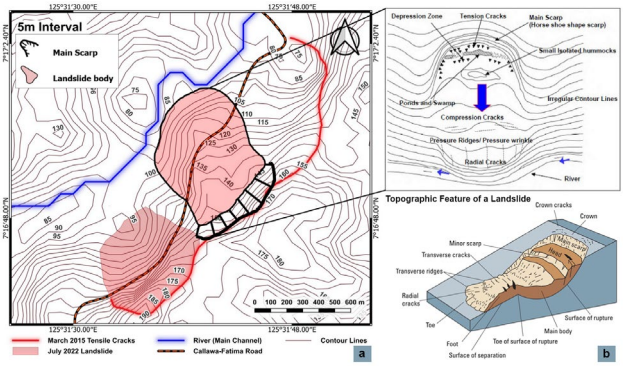

Fig. 12. Landslide topography (a) 5m Contour Interval VS (b) Topographic Feature of a Landslide (Photo Source: JICA 2012).

Importantly, these topographic features were preceded by clear precursors visible years earlier. Google Earth imagery from March 2015, as shown in Fig. 13, revealed a prominent tensile crack along the ridge crest that aligns directly with the crown of the July 2022 landslide. This continuity demonstrated that the 2015 crack was an incipient failure feature, which gradually propagated and weakened the slope until it ultimately collapsed seven years later. The imagery provided strong evidence of a long pre-failure history, underlining the value of historical remote sensing in identifying early warning signs.

Furthermore, Fig. 14 presents a time series of satellite imagery from August 2012 to May 2023, documenting the progressive geomorphic and anthropogenic changes at the Callawa–Fatima slope that led to the July 2022 landslide.

In 2012 (a), the slope was fully vegetated with no visible disturbances. By March 2015 (b), a prominent tensile crack had emerged along the ridge crest, representing the earliest visible sign of instability. Although vegetation largely recovered by July 2015 (c), bare soil patches at the crown suggested continued disturbance. The initiation of road concreting in April 2018 (d) introduced further slope modification. By 2019 (e) and 2021 (f), the road was fully constructed, while the slope still appeared vegetated and intact.

In February 2022 (g), imagery indicated subtle downslope displacement at the upper slope, though the area remained covered by vegetation, concealing the extent of ground deformation. The major transformation occurred by November 2022 (h), when the July 2022 landslide scarp was fully exposed, stripping vegetation and revealing the displaced mass. The imagery from May 2023 (i) showed the persistence of the failure zone, with disturbed ground extending downslope and limited natural recovery.

This time-lapse view made it clear that the slope did not fail suddenly, but rather evolved through years of subtle change. The first visible crack in 2015 was an early warning that the hillside was already weakening, even though vegetation later masked much of the disturbance. Road construction added further stress, and by 2022, the slope was primed for failure. When the heavy July rain arrived, they acted as the final trigger, exposing a landslide that had been silently developing for nearly a decade.

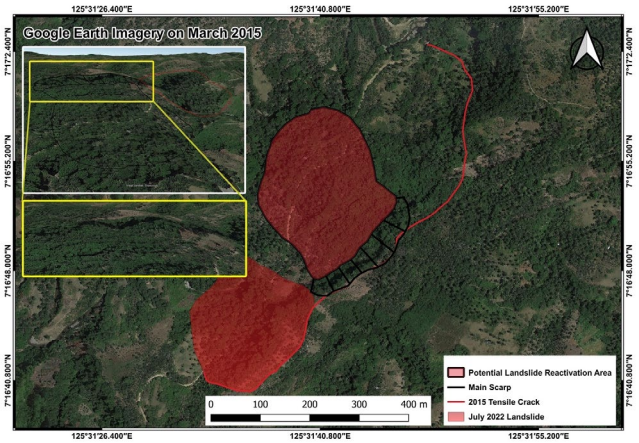

Fig. 13. Google Earth imagery from March 2015 Tensile Crack.

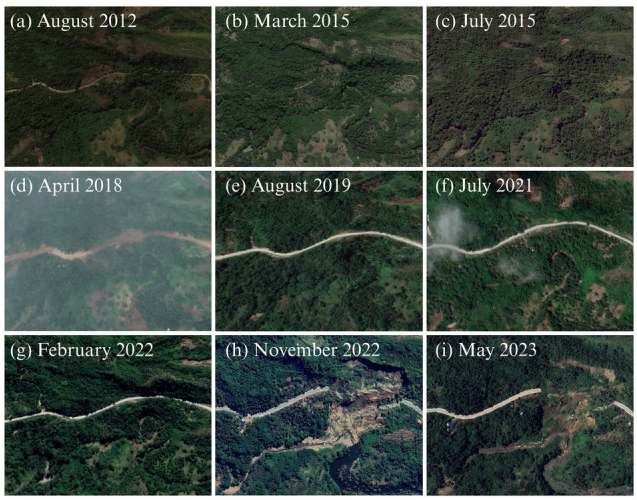

Fig. 14. Time series of satellite imagery from August 2012 to May 2023.

The Landslide Susceptibility Map (LSM), developed in QGIS through a Web Map Service (WMS) connection to the Philippine Geoportal, provided a broader context for the localized failures in the Callawa–Fatima area. The dataset

used originates from the National Mapping and Resource Information Authority (NAMRIA) and the Mines and Geosciences Bureau (MGB), which jointly produced the national Landslide Susceptibility Map. The LSM was accessed as an open-source WMS layer and overlaid with the study site's DEM-derived catchment and geomorphic features to assess correspondence with observed instability zones.

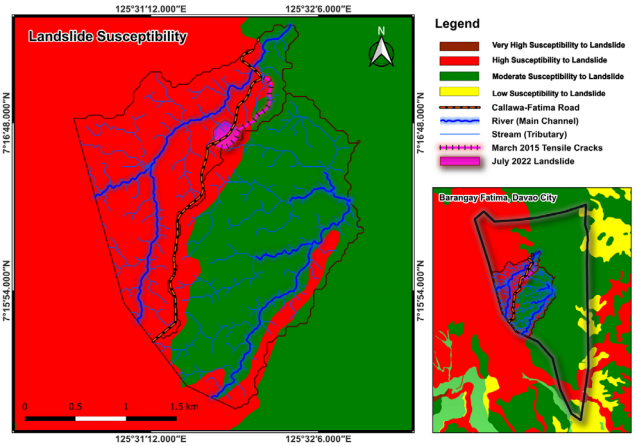

Fig. 15. Landslide susceptibility map.

As plotted in Fig. 15, the July 2022 landslide was situated within a zone classified as high susceptibility, consistent with the mapped hazard level. Similarly, the March 2015 tensile crack lay along a portion of moderate but mostly high-susceptibility corridor, signifying that both observed features fall within areas previously identified as prone to failure. At the catchment scale, a clear contrast was evident. Catchment Area 1, where the 2022 landslide occurred, was characterized by high susceptibility zones, whereas Catchment Area 2 was predominantly classified as having moderate susceptibility. This contrast reflected the influence of slope morphology and drainage concentration within the study site.

B. Numerical Modeling Results

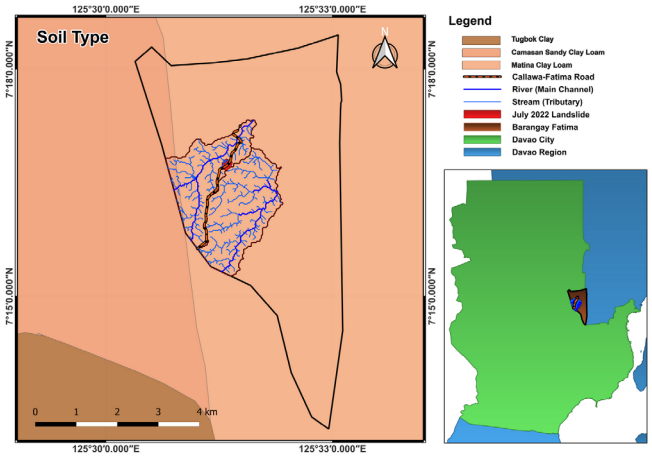

Fig. 16. Soil type map.

The numerical modeling was conducted in GEO5 to evaluate the slope stability of the Callawa–Fatima landslide section under varying hydrological conditions. Fig. 16 presents the soil type distribution across the study area, which validates that the 2022 landslide site was classified as a Matina Clay Loam, a soil unit classified under the Unified Soil Classification System (USCS), characterized as a clay with low to medium plasticity (CL, CI) and firm consistency. This classification is critical because such soils, while moderately cohesive, are prone to significant loss of strength upon saturation.

Table 2. Geotechnical parameters

Soil Type	Unit Weight, (kN/m^3)	Saturated Unit Weight, (kN/m^3)	Cohesion	Angle of Internal Friction
Clay with low or medium plasticity (CL, CI), firm consistency	18.00	19.50	12	20º

The geotechnical parameters adopted for the analysis are summarized in Table 2. The soil at the failure site was assigned with unit weights of 18.0 kN/m³ and 19.50 kN/m³, respectively, for its dry and saturated states. A cohesion value of 12 kPa and an internal friction angle of 20° were used to represent its shear strength. These values are characteristic of tropical residual clays, which possess moderate strength in unsaturated conditions but are highly sensitive to increases in pore water pressure. Under heavy or prolonged rainfall, the reduction in effective stress makes such soils prone to softening and shear failure, thereby lowering the overall slope stability.

1) Baseline dry-season condition

The baseline analysis under drained and unsaturated conditions provided an initial measure of slope stability prior to rainfall infiltration. As shown in Fig. 17, the computed Factors of Safety (FoS) vary along potential slip surfaces, with a maximum of 2.41 at the upper slope and a minimum of 0.87 near the road cut. A localized value of 1.35 was also observed along an intermediate slip surface.

These results highlighted the heterogeneous stability of the slope. While the upper portion remains relatively stable under dry-season conditions (FoS > 1.50), the mid-slope section near the road cut approached marginal stability (FoS ≈ 1.0). Importantly, the lowest FoS (<1.0) indicated that even in the absence of rainfall, critical zones of weakness already existed within the slope profile, particularly where road excavation altered the geometry.

2) Baseline wet-season condition

To represent rainfall infiltration and groundwater rise, a pore pressure coefficient (Ru = 0.40) was uniformly applied across the slope. This value falls within the conservative range of 0.2–0.5, commonly used for saturated clays in limit equilibrium analyses, ensuring that the model accurately reflects hydrological loading under intense rainfall conditions.

As shown in Fig. 18, the FoS declined markedly compared to the dry baseline scenario. The maximum FoS dropped to 1.66, while critical slip surfaces in the mid- and toe-slopes yielded values of 0.76 and 0.58, respectively. These results indicated that large sections of the slope transition into instability when pore pressures were introduced, with the road cut and lower slope being the most vulnerable zones, portraying global instability.

The sharp reduction in stability stressed the slope's sensitivity to hydrological forcing. While the slope retained marginal stability under unsaturated conditions, the introduction of pore pressure was sufficient to trigger large-scale instability. This behavior was consistent with field evidence from the July 2022 event, where progressive rainfall infiltration led to widespread cracking and ultimately failed.

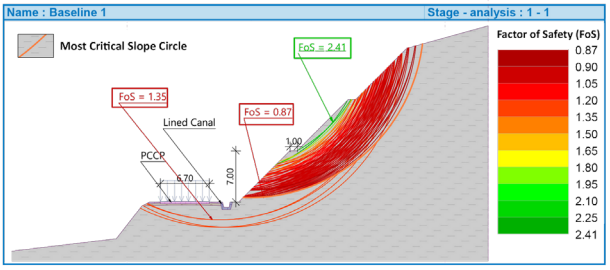

Fig. 17. Dry condition using Geo5 slope stability module.

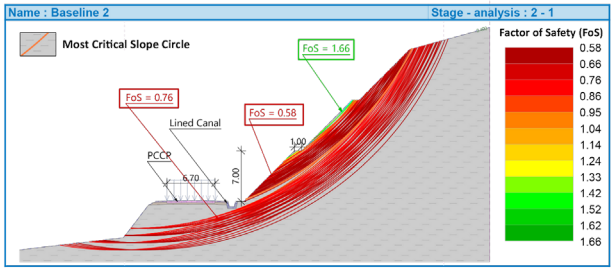

Fig. 18. Wet condition using Geo5 slope stability module.

C. Results of Household Vulnerability and Exposure Assessment

A Spatial Household Vulnerability and Exposure Assessment Map was developed, as shown in Fig. 19, to identify communities situated within areas potentially affected by slope-related hazards. The map shows resident dwellings located near the 2015 tensile crack and within the vicinity of the July 2022 failure zone. Several houses lie close to active scarps and along potential runout paths, underscoring their direct exposure to further slope movement.

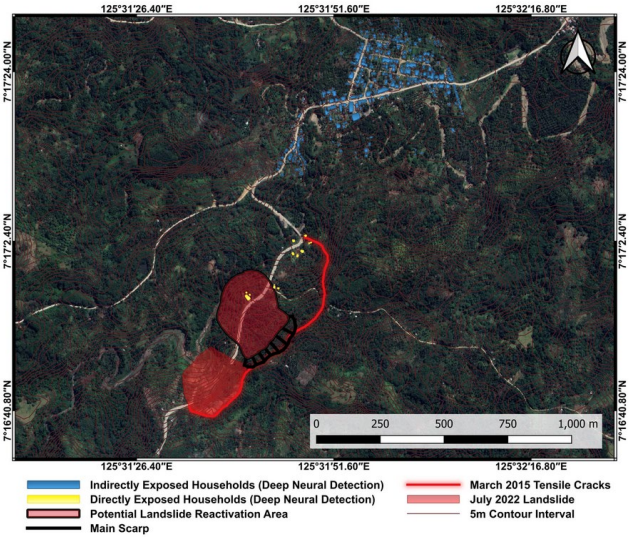

Fig. 19. Spatial household vulnerability and exposure assessment map.

All residential structures situated downslope of the March 2015 tensile cracks and within areas showing deformation indicators were classified as directly exposed. These households face immediate risk from continued slope movement, scarp expansion, or secondary landslides.

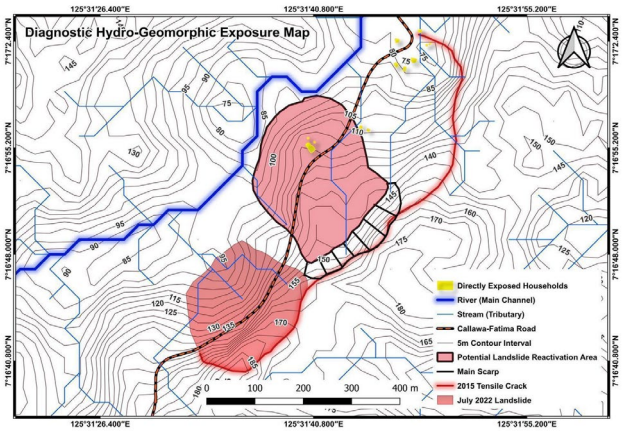

Fig. 20. Diagnostic Hydro-Geomorphic Exposure Map

In contrast, Barangay Fatima was classified as indirectly exposed, as it lay approximately 1 km downstream within the hydrological flow corridor of the Callawa–Fatima catchment. Although outside the current landslide footprint, reactivation of the 2022 failure or adjacent dormant slopes could generate a landslide-dam, whose blockage might trigger debris-flow surges and downstream sediment inundation. Table 3 summarizes the classification of household exposure and associated hazard processes.

Table 3. Classification of household exposure and associated hazard processes

Exposure Type	Spatial Criteria	Potential Hazard
Direct Exposure	Directly Exposed Households located within or immediately adjacent (≤100 m) to the 2015 tensile cracks, 2022 failure scarp, or geomorphic reactivation zones.	Secondary slope movement, ground subsidence, scarp retrogression, and localized debris slides.
Indirect Exposure	Barangay Fatima community (Indirectly Exposed Households) is located along the downstream flow corridor, hydrologically connected to the failure zone	River blockage by secondary landslides can cause landslide-dam formation and debris-flow surges or sediment inundation.

While this study focused primarily on physical exposure, socio-economic parameters, such as household income, adaptive capacity, and coping mechanisms, were not incorporated into the present hydro-geomorphic diagnostic. This exclusion was justified by the study's emphasis on physical process diagnosis and spatial exposure delineation, where reliable socio-economic data were not yet available at the parcel scale.

D. Integrated Discussion

The July 2022 Callawa–Fatima landslide resulted from the interaction of hydrological, geomorphic, and geotechnical processes. PAGASA rainfall records show that several days of moderate wetting (July 8–12) preconditioned the slope, while intense bursts on July 13–14 sharply increased pore pressures. Field evidence confirmed this sequence: community reports of cracking on July 10 coincided with

antecedent rainfall, and inspection teams later observed ground movement before the collapse. These hydrological triggers acted on a slope that was already predisposed to failure, as indicated by geomorphic analyses. The 2015 tensile crack, the contour distortions, and vegetation changes over time all signaled progressive weakening. Similar behavior was reported by Kolathayar, Menon, and Kundu [53], who analyzed the July 2024 landslide in Wayanad, India, where continuous antecedent rainfall over 48 h induced debris flow and slope reactivation along steep convergent catchments. This supported the present study's finding that short-duration, high-intensity rainfall, when superimposed on already saturated slopes, can initiate deep-seated movement.

LEM modeling further validated this progression, showing that even under dry-season conditions, localized slip circles near the road canal yielded FoS values below 1.0, indicating partial instability. In contrast, the introduction of pore pressure led to larger sections of the slope experiencing full slope failure (FoS < 0.58).

The implications extend beyond the 2022 landslide. Geomorphic and susceptibility mapping reveal that the adjacent slope west of the main failure zone displays the classic topographic features of an inactive landslide body, intersected upslope by a stream tributary and undercut downslope by the river. This area is not only geomorphically unstable but also socially vulnerable: several households are located above and below the slope, while further downslope, the community of Barangay Fatima lies along the same corridor, preceded by a bridge that crosses the river. These interacting hydrological and geomorphic processes are illustrated in Fig. 20, the Diagnostic Hydro-Geomorphic Exposure Map.

IV. Conclusion and Recommendations

A. Conclusion

The Callawa–Fatima landslide of July 2022 has demonstrated the combined influence of long-term preconditioning and short-term hydrological forcing in a tropical mountain region. Field and historical records documented tensile cracks as early as 2015, while 5m contour analysis and landslide susceptibility mapping confirmed the presence of both active and dormant instability features. Hydrological assessment showed that Catchment Area 1 directs drainage flows into the landslide zone, and that days of antecedent wetting followed by high-intensity rainfall bursts substantially increased pore water pressures. Numerical modeling indicated that hydrological loading further decreased the already marginal stability under dry conditions, reducing the Factor of Safety to values significantly below 1.0 under wet conditions.

This study establishes a hydro-geomorphic diagnostic framework using freely available datasets and accessible analytical tools, making it well suited for data-scarce and resource-limited settings. Although the analysis is constrained by the resolution of the ASTER DEM, reliance on rainfall data from a single PAGASA station, and the use of estimated soil parameters due to the absence of in-situ monitoring, the framework effectively identified key instability mechanisms and high-risk zones. As such, it provides a practical and transferable basis for diagnosing rainfall-induced slope failures, supporting early warning efforts, and enhancing the resilience of road infrastructure and nearby communities in tropical mountainous regions.

B. Recommendations

Effective slope risk management in the Callawa–Fatima Road network requires an integrated approach that combines hydrological threshold-based early warning, continuous geomorphic monitoring, and engineered stabilization measures tailored to clay-rich tropical soils. Specifically:

1) Implement continuous monitoring of tensile cracks and nearby dormant landslide zones using field instruments like extensometers, inclinometers, and localized rain gauges and remote sensing techniques.
2) Develop rainfall-threshold-based early warning systems using PAGASA data supplemented by on-site rain gauges, with consideration of future climate-driven rainfall intensification.
3) Integrate gray and green infrastructure, including drainage, retaining structures, Mechanically Stabilized Earth (MSE) walls, and vegetation-based erosion control, to enhance slope stability and hydrological resilience.
4) Adopt risk-sensitive land-use planning for exposed households and downstream infrastructure, supported by community-based preparedness and evacuation measures.
5) Balance cost-effectiveness and long-term risk reduction in post-failure road rehabilitation by stabilizing the distressed slope must still be considered to protect nearby households, the Barangay Fatima community, and the downstream bridge from secondary slope failures or sediment mobilization along the river corridor.

Conflict of Interest

The authors declare that they have no known competing financial interests or personal relationships that could have appeared to influence the work reported in this paper.

Author Contributions

Lester G. Padilla conducted the research, including conceptualization, methodology design, field investigation, data curation, and formal analysis. He also executed the software workflows, performed the visualization, and prepared the original manuscript draft. Eleonor V. Palconit supervised the overall study, validated the analyses, and contributed to the review and editing of the final manuscript. Both authors have read and approved the final version of the paper.

Acknowledgment

The authors wish to thank the faculty of the School of Engineering and Architecture at Ateneo de Davao University for their academic support and technical guidance throughout the preparation of this manuscript. Special appreciation is extended to colleagues who provided insights on regional slope hazards and data accessibility in the Philippines.

References

[1] S. Pradhan, D. G. Toll, N. J. Rosser, and M. J. Brain, "An investigation of the combined effect of rainfall and road cut on landsliding," *Eng Geol*, vol. 307, 106787, 2022. doi: 10.1016/j.enggeo.2022.106787

[2] G. Jiménez-Ramos, T. Echaveguren, J. Vargas-Baecheler, and A. Chamorro, "Traffic interruption risk induced by cut-slope failure: The rainfall effect," *Transportation Geotechnics*, vol. 41, 100993, 2023. doi: 10.1016/j.trgeo.2023.100993

[3] N. L. J. Dolojan, S. Moriguchi, M. Hashimoto, N. X. Tinh, H. Tanaka, and K. Terada, "Hydrologic-geotechnical modelling of shallow landslide and flood hazards caused by heavy rainfall," *Eng Geol*, vol. 323, 107184, 2023. doi: 10.1016/j.enggeo.2023.107184

[4] W. H. Schulz, G. Wang, Y. Jiang, B. D. Collins, M. E. Reid, and M. M. Einbund, "Shear surface undulations modulate clayey gouge strength and contribute to divergent landslide acceleration," *Eng Geol*, vol. 357, 108353, 2025. doi: 10.1016/j.enggeo.2025.108353

[5] A. Vitaletti, E. Cernuto, and D. Salciarini, "Coupling finite element modelling and InSAR data for enhanced understanding of landslide behaviour along highway infrastructures," *Landslides*, 2025. doi: 10.1007/s10346-025-02610-y

[6] E. Alcântara, C. F. Baião, Y. C. Guimarães, J. A. Marengo, and J. R. Mantovani, "Climate change-induced shifts in landslide susceptibility in São Sebastião (southeastern Brazil)," *Natural Hazards Research*, 2025. doi: 10.1016/j.nhres.2024.11.005

[7] Z. Fang, A. B. Morales, Y. Wang, and L. Lombardo, "Climate change has increased rainfall-induced landslide damages in central China," *International Journal of Disaster Risk Reduction*, vol. 119, 105320, 2025. doi: 10.1016/j.ijdrr.2025.105320

[8] C. Abanco, G. L. Bennett, A. J. Matthews, M. Anthony, M. Matera, and F. J. Tan, "The role of geomorphology, rainfall and soil moisture in the occurrence of landslides triggered by 2018 Typhoon Mangkhut in the Philippines," *Natural Hazards and Earth System Sciences*, vol. 21, pp. 1531–1550, 2021. doi: 10.5194/nhess-21-1531-2021

[9] H. G. Smith, A. J. Neverman, H. Betts, and R. Spiekermann, "The influence of spatial patterns in rainfall on shallow landslides," *Geomorphology*, vol. 437, 108795, 2023. doi: 10.1016/j.geomorph.2023.108795

[10] I. Alcántara-Ayala, "Landslides in a changing world," *Landslides*, 2025. doi: 10.1007/s10346-024-02451-1

[11] H. A. Mirdda, S. Bera, and R. Chatterjee, "Vulnerability assessment of mountainous households to landslides: A multidimensional study in the rural Himalayas," *International Journal of Disaster Risk Reduction*, vol. 71, 102809, 2022. doi: 10.1016/j.ijdrr.2022.102809

[12] R. S. Yanquiling, "Predictors of risk reduction behavior: Evidence in last-mile communities," *International Journal of Disaster Risk Reduction*, vol. 113, 104875, 2024. doi: 10.1016/j.ijdrr.2024.104875

[13] C. J. Cordero, K. Gesmundo, and A. Daag, "Assessing and contextualizing site-specific landslide risk in the Philippines," in *Proc. Landslide Risk and Disaster Resilience*, pp. 149–162, 2025. doi: 10.1007/978-3-031-72736-8_12

[14] O. Varun Menon and S. Kolathayar, "Enhancing disaster preparedness in mountainous regions: A review of IoT and machine learning techniques," in *Proc. Lecture Notes in Civil Engineering*, vol. 589, pp. 15–29, Springer Science and Business Media Deutschland GmbH, 2025. doi: 10.1007/978-981-96-3220-6_2

[15] Y. Peiro, E. Volpe, L. Ciabatta, and E. Cattoni, "High resolution precipitation and soil moisture data integration for landslide susceptibility mapping," *Geosciences (Switzerland)*, vol. 14, no. 12, 330, 2024. doi: 10.3390/geosciences14120330

[16] M. Kühnl, M. Sapena, M. Wurm, C. Geiß, and H. Taubenböck, "Multitemporal landslide exposure and vulnerability assessment in Medellín, Colombia," *Natural Hazards*, vol. 119, pp. 883–906, 2023. doi: 10.1007/s11069-022-05679-z

[17] B. Azmoon, A. Biniyaz, and Z. Liu, "Use of high-resolution multi-temporal DEM data for landslide detection," *Geosciences (Switzerland)*, vol. 12, no. 10, 378, 2022. doi: 10.3390/geosciences12100378

[18] Á. M. Moreno-Pájaro *et al.*, "Hydrological modelling and remote sensing for assessing the impact of vegetation cover changes," *Hydrology*, vol. 12, no. 5, 107, 2025. doi: 10.3390/hydrology12050107

[19] R. Coluzzi *et al.*, "Rapid landslide detection from free optical satellite imagery using a robust change detection technique," *Scientific Reports*, vol. 15, 1221, 2025. doi: 10.1038/s41598-025-89542-8

[20] J. Thomas, M. Gupta, P. K. Srivastava, and G. P. Petropoulos, "Assessment of a dynamic physically based slope stability model to evaluate timing and distribution of rainfall-induced shallow landslides," *ISPRS International Journal of Geo-Information*, vol. 12, no. 3, 105, 2023. doi: 10.3390/ijgi12030105

[21] G. Amatulli *et al.*, "Hydrography90m: A new high-resolution global hydrographic dataset," *Earth System Science Data*, vol. 14, pp. 4525–4550, 2022. doi: 10.5194/essd-14-4525-2022

[22] R. Rochmawati, P. H. Sitorus, and I. Irianto, "Slope stability analysis using GEO5 in Gurabesi Village Papua Province based on limit equilibrium method," in *Proc. AIP Conference Proceedings*, vol. 3145, 2024. doi: 10.1063/5.0214559

[23] A. Anand and A. Anand, "Fusion of terrestrial laser scanning and UAV photogrammetry for advanced landslide monitoring: Integrated assessment of the Kshetrapal landslide, Chamoli district, Uttarakhand, India," *International Journal of Geosciences*, vol. 16, pp. 464–504, 2025. doi: 10.4236/ijg.2025.167023

[24] P. Sestras *et al.*, "A novel method for landslide deformation monitoring by fusing UAV photogrammetry and LiDAR data based on each sensor's mapping advantage in regards to terrain feature," *Eng Geol*, vol. 346, 107890, 2025. doi: 10.1016/j.enggeo.2024.107890

[25] B. Chen, J. Maurer, and W. Gong, "Applications of UAV in landslide research: A review," *Landslides*, 2025. doi: 10.1007/s10346-025-02547-2

[26] J. J. Lee, M. S. Song, H. S. Yun, and S. G. Yum, "Dynamic landslide susceptibility analysis that combines rainfall period, accumulated rainfall, and geospatial information," *Scientific Reports*, vol. 12, 18429, 2022. doi: 10.1038/s41598-022-21795-z

[27] M. Abrams, R. Crippen, and H. Fujisada, "ASTER Global Digital Elevation Model (GDEM) and ASTER Global Water Body Dataset (ASTWBD)," *Remote Sensing*, vol. 12, no. 7, 1156, 2020. doi: 10.3390/rs12071156

[28] V. E. Johnston, F. Šarc, K. Wątor, and B. Otoničar, "Hydrogeochemical data from carbonate springs as an aid for delimiting catchment areas in the Rovte region, Central Slovenia," *Journal of Hydrology: Regional Studies*, vol. 56, 102087, 2024. doi: 10.1016/j.ejrh.2024.102087

[29] H. Han, Q. Zeng, and J. Jiao, "Quality assessment of tandem-x dems, srtm and aster gdem on selected chinese sites," *Remote Sensing*, vol. 13, no. 7, 1304, 2021. doi: 10.3390/rs13071304

[30] S. Gameiro, G. G. de Oliveira, and L. A. Guasselli, "The influence of sampling on landslide susceptibility mapping using artificial neural networks," *Geocarto International*, 2022. doi: 10.1080/10106049.2022.2144475

[31] M. Conforti, M. Mercuri, and L. Borrelli, "Morphological changes detection of a large earthflow using archived images, lidar-derived dtm, and uav-based remote sensing," *Remote Sensing*, vol. 13, no. 1, 120, 2021. doi: 10.3390/rs13010120

[32] T. Shukla, W. Tang, C. C. Trettin, G. Chen, S. Chen, and C. Allan, "Quantification of microtopography in natural ecosystems using close-range remote sensing," *Remote Sensing*, vol. 15, no. 9, 2387, 2023. doi: 10.3390/rs15092387

[33] S. M. Luglio *et al.*, "A biodiversity monitoring case study in viticulture: Manual and digitalized collaborative methodology to pursue the European Commission's sustainable challenges," *Sustainability*, vol. 16, no. 8, 3469, 2024. doi: 10.3390/su16083469

[34] D. L. D. Aschieri, N. Sobrino, and E. Macii, "Web-GIS application for hydrogeological risk prevention: The case study of Cervo Valley," *Sustainability*, vol. 16, no. 22, 9833, 2024. doi: 10.3390/su16229833

[35] M. Uzielli, A. Geppetti, L. Borselli, S. Renzi, and F. Preti, "Comparative geotechnical analysis of slope stabilization through conventional, soil and water bioengineering, and combined solutions," *Ecological Engineering*, vol. 212, 107487, 2025. doi: 10.1016/j.ecoleng.2024.107487

[36] N. Monte *et al.*, "A dataset of geotechnical parameters based on international literature to characterise lithotypes in Italy," *Scientific Data*, vol. 11, 1177, 2024. doi: 10.1038/s41597-024-04095-1

[37] A. Alok, A. Burman, P. Samui, M. R. Kaloop, and M. Eldessouki, "A generalized limit equilibrium-based platform incorporating simplified Bishop, Janbu and Morgenstern–Price methods for soil slope stability problems," *Advances in Civil Engineering*, vol. 2024, 3053923, 2024. doi: 10.1155/2024/3053923

[38] B. S. Firincioglu and M. Ercanoglu, "Insights and perspectives into the limit equilibrium method from 2D and 3D analyses," *Eng Geol*, vol. 281, 105968, 2021. doi: 10.1016/j.enggeo.2020.105968

[39] M. P. Amarasinghe, D. Robert, S. A. S. Kulathilaka, A. Zhou, and H. A. G. Jayathissa, "Slope stability analysis of unsaturated colluvial slopes based on case studies of rainfall-induced landslides," *Bulletin of Engineering Geology and the Environment*, vol. 83, p. 171, 2024. doi: 10.1007/s10064-024-03933-1

[40] R. Ullah, R. A. Abdullah, A. Kassim, N. Z. M. Yunus, and H. Sendo, "Assessment of residual soil properties for slope stability analysis," *International Journal of GEOMATE*, vol. 21, no. 86, pp. 72–80, 2021. doi: 10.21660/2021.86.j2282

[41] D. Sarah *et al.*, "Back analysis of rainfall-induced landslide in Cimanggung District of Sumedang Regency in West Java using deterministic and probabilistic analyses," *Geosciences (Switzerland)*, vol. 14, no. 12, 347, 2024. doi: 10.3390/geosciences14120347

[42] F. Ahmad, P. Kumar, D. R. Kumar, W. Wipulanusat, and P. Samui, "Geotechnical evaluation of embankment stability in seismic zones

using Monte Carlo and subset simulations within an LRFD framework aided by machine learning," *Results in Engineering*, vol. 27, 106320, 2025. doi: 10.1016/j.rineng.2025.106320

[43] S. Wu, S. Huang, L. Han, C. Wang, M. Ren, and H. Shen, "Chart-based slope stability assessment using the slope shape influence factor," *Results in Engineering*, vol. 26, 105603, 2025. doi: 10.1016/j.rineng.2025.105603

[44] W. Ouyang, S. W. Liu, and Y. Yang, "An improved Morgenstern-Price method using Gaussian quadrature," *Computers and Geotechnics*, vol. 148, 104754, 2022. doi: 10.1016/j.compgeo.2022.104754

[45] D. Singh and V. Kumar, "Slope stability analysis of highway embankment by using GEO5 software," in *Proc. Lecture Notes in Civil Engineering*, vol. 280, pp. 249–257, Springer Science and Business Media Deutschland GmbH, 2023. doi: 10.1007/978-981-19-4739-1_24

[46] L. Luo, P. Li, and X. Yan, "Deep learning-based building extraction from remote sensing images: A comprehensive review," *Energies*, vol. 14, no. 23, 7982, 2021. doi: 10.3390/en14237982

[47] R. A. Emberson, D. B. Kirschbaum, and T. Stanley, "Landslide hazard and exposure modelling in data-poor regions: The example of the Rohingya refugee camps in Bangladesh," *Earth's Future*, vol. 9, no. 9, 2021. doi: 10.1029/2020EF001666

[48] Y. Wang, H. Wen, D. Sun, and Y. Li, "Quantitative assessment of landslide risk based on susceptibility mapping using random forest and geodetector," *Remote Sensing*, vol. 13, no. 13, 2625, 2021. doi: 10.3390/rs13132625

[49] Y. Tang *et al.*, "Assessing debris flow risk at a catchment scale for an economic decision based on the LiDAR DEM and numerical simulation," *Frontiers in Earth Science*, vol. 10, 2022. doi: 10.3389/feart.2022.821735

[50] P. Aszkowski, B. Ptak, M. Kraft, D. Pieczyński, and P. Drapikowski, "Deepness: Deep neural remote sensing plugin for QGIS," *SoftwareX*, vol. 23, 101495, 2023. doi: 10.1016/j.softx.2023.101495

[51] R. A. C. Garcia, S. C. Oliveira, and J. L. Zêzere, "Assessing population exposure for landslide risk analysis using dasymetric cartography," *Natural Hazards and Earth System Sciences*, vol. 16, pp. 2769–2782, 2016. doi: 10.5194/nhess-16-2769-2016

[52] R. Chang, J. Wang, L. Li, and D. Chen, "Extraction and analysis of the spatial morphology of a heritage village based on digital technology and weakly supervised point cloud segmentation methods: An innovative application in the case of Xisongbi Village in Jiexiu City, Shanxi Province," *Sustainability*, vol. 17, no. 8, 3349, 2025. doi: 10.3390/su17083349

[53] S. Kolathayar, V. Menon, and P. Kundu, "Landslides and debris flow triggered by the July 2024 extreme rainstorm in the Chooralmala watershed in Wayanad, India," *Landslides*, vol. 22, pp. 967–974, 2025. doi: 10.1007/s10346-024-02443-1